2013-01-07

Luminescent LaF_3:Ce-Doped Organically Modified Nanoporous Silica Xerogels

UTD AUTHOR(S): Ning Lu, Jinguo Wang, Huiyang Luo, Moon J. Kim and Hongbing Lu

Luminescent LaF_3:Ce-doped organically modified nanoporous silica xerogels

Mingzhen Yao,[1] Ryan Hall,[1] Wei Chen,[1,a)] Dhairyashil P. Mohite,[2] Nicholas Leventis,[2] Ning Lu,[3] Jinguo Wang,[3] Moon J. Kim,[3] Huiyang Luo,[4] and Hongbing Lu[4]
[1]*Department of Physics, The University of Texas at Arlington, Arlington, Texas 76019-0059, USA*
[2]*Department of Chemistry, Missouri University of Science and Technology, Rolla, Missouri 65409, USA*
[3]*Department of Materials Science and Engineering, The University of Texas at Dallas, Richardson, Texas 75080, USA*
[4]*Department of Mechanical Engineering, The University of Texas at Dallas, Richardson, Texas 75080, USA*

(Received 5 September 2012; accepted 10 December 2012; published online 7 January 2013)

Organically modified silica compounds (ORMOSILs) were synthesized by a sol-gel method from amine-functionalized 3-aminopropyl triethoxylsilane and tetramethylorthosilicate and were doped *in situ* with LaF_3:Ce nanoparticles, which in turn were prepared either in water or in ethanol. Doped ORMOSILs display strong photoluminescence either by UV or X-ray excitation and maintain good transparency up to a loading level of 15.66% w/w. The TEM observations demonstrate that ORMOSILs remain nanoporous with pore diameters in the 5–10 nm range. LaF_3:Ce nanoparticles doped into the ORMOSILs are rod-like, 5 nm in diameter and 10–15 nm in length. Compression testing indicates that the nanocomposites have very good strength, without significant lateral dilatation and buckling under quasi-static compression. LaF_3:Ce nanoparticle-doped ORMOSILs have potential for applications in radiation detection and solid state lighting. © *2013 American Institute of Physics*. [http://dx.doi.org/10.1063/1.4773330]

I. INTRODUCTION

For radiation detection, sensitivity, response time, and energy resolution are important factors. To perform optimally, a scintillator must have a high luminescence quantum efficiency, a fast decay time, and a high stopping power for radiation beams, as well as high carrier mobility-lifetime products.[1] In nanoparticles, due to size confinement, the spatial distribution of the luminescence centers and carriers is confined within the particles, the probability of energy transfer from carriers to the luminescent centers is increased, and therefore the emission efficiency is enhanced.[2,3] Furthermore, due to quantum size confinement and the increased overlap of electron and hole wave functions, nanoparticles can have greater luminescence efficiency than that of the corresponding bulk materials.[4,5] Thus, scintillation nanoparticles, in principle, can have enhanced light output (i.e., luminescence efficiency) with faster response, which is promising for radiation detection. Experimentally, it has been observed that scintillation nanoparticles have advantages over bulk scintillators for radiation detection.[6] Scintillating nanoparticles based on bulk scintillators have been shown to possess three times higher luminescence efficiency[6] and double the energy resolution,[7] as compared to their bulk crystal analogs.

For practical applications, nanoparticles work best for radiation detection when they are in the form of films, gels, or crystals. A simple and effective way to achieve those forms is to encapsulate nanoparticles in polymers to form bulk nanocomposite materials. High quality bulk nanocomposite thin films with high scintillation luminescence and high transparency will have potential to complement and even potentially replace single crystals for radiation detection. In this paper, we investigate the structural, physical, and luminescence properties of LaF_3:Ce-doped ORganically MOdified SILica (ORMOSIL), with respect to their potential application for radiation detection. The sol-gel process is a facile and consistent method to synthesize films and bulk "crystals." In the past two decades, sol-gel science has been concentrated primarily on inorganic oxides.[8] In general, the sol-gel process consists of hydrolysis and condensation reactions, in which alkoxysilanes such as tetramethoxysilane (TMOS) or tetraethoxysilane (TEOS), are mixed with water in a mutual solvent like methanol or ethanol.[9,10] Doping of silica xerogels with nanoparticles has gained increasing interest since the sol-gel method starts from a homogeneous solution, which gives a better control over distribution and properties of nanoparticles embedded within the silica matrix.[11–15] However, silica xerogels produced via a conventional sol-gel process are generally brittle and stiff since the nano-porous structure collapses to a dense structure due to capillary forces during ambient pressure drying.[16] ORMOSILs have been considered as a better solid matrix due to their flexibility, permeability, and porosity by incorporating organics into sol-gel-derived silica.[9,17] ORMOSIL bulk and powder materials doped with nanoparticles have been found to be good phosphors with high relative emission intensity.[11–15,18] In that regard, Ce^{3+}-doped nanoparticles have found numerous applications in radiation detection and dosimetry, with applications in medical imaging systems and diagnostic radiology.[19–26] In this paper, we report the synthesis, structure, and mechanical and optical properties of LaF_3:Ce-doped ORMOSILs, and then discuss their potential applications for radiation detection.

a)Author to whom correspondence should be addressed. Electronic mail: weichen@uta.edu.

II. EXPERIMENTAL SECTION

A. Materials

Lanthanum (III) nitrate hydrate ($La(NO_3)_3 \cdot H_2O$, 99.9%), cerium (III) nitrate hexahydrate ($Ce(NO_3)_3 \cdot 6H_2O$ 99.9%), ammonium fluoride (NH_4F, 99.9%), poly(ethylene glycol) bis(carboxymethyl), ethanol, TMOS, 3-aminopropyltriethoxysilane (APTES), and nitric acid (HNO_3) were purchased from Sigma-Aldrich and were used as received.

B. Methods

1. Synthesis of water- and ethanol-soluble LaF_3:Ce

LaF_3:Ce nanoparticles were synthesized by two different methods, referenced as water-based and ethanol-based nanoparticles, respectively. To form a water-based LaF_3:Ce solution, 3.52 mmol of $La(NO_3)_3$ and 0.88 mmol of $Ce(NO_3)_3 \cdot 6H_2O$ were first dissolved in 15 ml of de-ionized water. Polyethyleneglycol (PEG, 1 ml) was added to the above solution as stabilizer. After those reagents were dissolved completely, 14 mmol of NH_4F dissolved in 5 ml of water was added dropwise to the solution under stirring at room temperature. The reaction mixture was stirred at room temperature for 0.5 h under N_2 and was subsequently heated to 50 °C for 2 h. The product was centrifuged, washed with de-ionized water three times, dried at 40 °C in a vacuum atmosphere, and was re-dispersed into 20 ml of de-ionized water. Similarly, an ethanol-based solution of LaF_3:Ce nanoparticles was synthesized by substituting water with ethanol in the above procedure. Due to the different solubility of LaF_3:Ce nanoparticles in water and ethanol, the concentrations of solutions were 0.22 M for water-based nanoparticles and 0.16 M for ethanol-based nanoparticles.

2. Synthesis of amine modified ORMOSILs

The ORMOSILs of this study were synthesized via a sol-gel process. Hydrolysis and polycondensation associated with that process are reactions of metal-organic compounds, such as silicon alkoxides (TMOS, or TEOS) with water catalyzed by acid or base. In the case of inorganic–organic hybrid systems (ORMOSILs), the silicate network is modified with organic groups (e.g., methyl, ethyl, 3-glycidoxypropyl, 3-isocyanatopropyl, etc.) by copolymerization of TMOS or TEOS and an appropriately functionalized silane. In our case, we used copolymerization of TMOS and APTES according to a modified literature procedure to obtain silica whose surface is modified with amines.[14,15] For this, two solutions were prepared separately, one consisting of 11 ml of TMOS, 2 ml of de-ionized water, 25 ml of ethanol, and 0.155 ml of HNO_3 (solution A), and the other one consisting of 2 ml of APTES and 10 ml of ethanol (solution B). Solution A was stirred thoroughly in a beaker for 30 min to initialize the hydrolysis process, then solution B was added to it and the mixture was mixed rapidly. The resulting sol was poured into polyethylene syringes (5 ml) used as molds, whose open ends were covered with three layers of Parafilm™. Gelation takes place in about 3 s to 5 min after mixing solution A with solution B, and the gelation time varied with the level of doping (see below). After aging (5 h), we punched a small pinhole in the Parafilm™ cover, and we added a new pinhole every two days afterwards. Dry gels (xerogels) were obtained after 15 days.

3. Synthesis of LaF_3:Ce doped ORMOSILs

To dope LaF_3:Ce nanoparticles into ORMOSILs, we used two different sources of nanoparticles: water-based LaF_3:Ce and ethanol-based LaF_3:Ce prepared as described in previous section. For the first set of samples (with water-based LaF_3:Ce nanoparticles), we substituted the corresponding amount of de-ionized water of solution A with the solution of the water-based nanoparticles. Four LaF_3:Ce-doped ORMOSILs with different doping concentrations were synthesized (0.001964 M, 0.0039 M, 0.0059 M, and 0.0078 M). The second set of samples were synthesized using the ethanol-based LaF_3:Ce nanoparticles as the doping source. Similarly, portions of ethanol in solution A used for the ORMOSIL synthesis were substituted with the ethanol-based LaF_3:Ce nanoparticle solution. Accordingly, another set of four LaF_3:Ce-doped ORMOSILs were synthesized with different doping concentrations (0.0145 M, 0.029 M, 0.0435 M, and 0.058 M).

C. Characterization of nanoparticle doped ORMOSILs

The identity, crystalline structure, size, and shape of the nanoparticles were determined with X-ray diffraction, scanning electron microscope (SEM), and high resolution transmission electron microscopy (HRTEM). Chemical component analysis of ORMOSILs was performed by electron energy loss spectra (EELS). The X-ray powder diffraction (XRD) patterns of LaF_3:Ce doped ORMOSILs were recorded in the range of $20° \leq 2\theta \leq 80°$ using a Siemens Kristalloflex 810 D-500 X-ray diffractometer operating at 40 kV and 30 mA with a radiation beam of $\lambda = 1.5406$ Å. For HRTEM, the nanocomposites suspended in ethanol were brought onto microperforated carbon covered copper grids. HRTEM images and EELS were obtained using a JEOL JEM-2100 F transmission electron microscope operated at 200 kV. UV-excitation and emission spectra were recorded using a Shimadzu RF-5301PC fluorescence spectrophotometer. The samples were exposed to X-ray excitation using a home-built X-ray chamber. The chamber is equipped with an Oxford Instruments XTF5011 X-ray tube with a tungsten target, and the X-ray tube was operated at 50 kVp and 1 mA. Emission spectra obtained with X-ray excitation were recorded using fiber optic cables connected to a fluorescence spectrometer (Ocean Optics).

Surface areas and pore size distributions were measured by nitrogen sorption porosimetry using a Micromeritics ASAP 2020 surface area and porosity analyzer. Sample preparation included outgassing for 24 h under vacuum at 80 °C. Average pore diameters were determined by the $4 \times V_{Total}/\sigma$ method, where V_{Total} is the total pore volume per gram of sample and σ, the surface area was determined by the Brunauer-Emmett-Teller (BET) method from the N_2 adsorption isotherm. The value of V_{Total} was obtained from the single highest volume of N_2 adsorbed along the adsorption isotherm. Average pore

diameter values were also calculated using the Barret-Joyner-Halenda (BJH) equation applied on both the adsorption and desorption branches of the isotherms.

1. Compression testing

Compression testing was performed according to the ASTM D695-02 a standard on cylindrical specimens, using an Instron machine (Model 5567 A) equipped with a 30 kN load cell. According to the ASTM standard, the height to diameter ratio of the specimen should be 2:1. Samples used for mechanical testing were dry-cut without using any lubrication liquid on a low speed diamond saw (MTI Corporation, SYJ-150 A). The cut surfaces of the samples were slightly polished using grade 600 fine silicon carbide sandpaper to make both end surfaces flat and parallel to each other. The bottom surface was held stationary whereas the top cross-head descended at a speed of about 0.152 mm/min. The load was measured with a compression load cell, and the displacement data were directly determined from the crosshead movement. Compression tests were conducted at room temperature and ~35% humidity. The load-displacement curve for each test was converted to a stress-strain curve by dividing the load by the original cross-sectional area of the specimen (average cross-sectional area of the specimens was 31.67 mm^2) and the displacement by the height of the specimens (average height of the specimens was 12.7 mm). The compressive stress at ultimate failure, the strain at failure, and the Young's modulus were extracted from the stress-strain curves. The strain at failure was the strain at which the macroscopic failure of the specimen occurred. Samples were loaded at quasi-static strain rates of 0.0002 per second.

III. RESULTS AND DISCUSSION

ORMOSILs are very sensitive to the ratio of the reagents. A change of that ratio may cause cracking or produce an opaque sample. Figure 1 shows pure ORMOSIL samples without any doping. They are transparent, which is a favorable characteristic for radiation detection.

ORMOSILs were doped with water-based and ethanol-based LaF_3:Ce nanoparticles, respectively. The original molar doping concentrations in the LaF_3:Ce@ORMOSIL samples were 0.001964 M, 0.0039 M, 0.0059 M, and 0.0078 M for water-based LaF_3:Ce nanoparticles, and 0.0145 M, 0.029 M, 0.0435 M, and 0.058 M for ethanol-based LaF_3:Ce nanoparticles. By converting the molar nanoparticle concentration into weight percentage loading level, the nanoparticle loading levels in the LaF_3:Ce@ORMOSIL samples doped with water-based LaF_3:Ce nanoparticles were 3.63% (HA), 7.01% (HB), 10.17% (HC) and 13.11% (HD) w/w, and 15.66% (EA), 27.09% (EB), 35.78% (EC), and 42.63% (ED) w/w for the LaF_3:Ce@ORMOSIL samples made with ethanol-based nanoparticles. Figure 2 shows LaF_3:Ce@ORMOSIL samples doped with water-based LaF_3:Ce, where nanoparticle loading increases from 3.63% w/w on the left to 13.11% w/w on the right. All samples are transparent except those with the highest loading concentration of 13.11% w/w (HD). It indicates that nanoparticle loading using water-based LaF_3:Ce could reach levels up to somewhere between 10.17% and 13.11% w/w, and maintain good transparency. LaF_3:Ce@ORMOSIL samples doped with ethanol-based LaF_3:Ce are shown in Figure 3. As the nanoparticle loading levels in those samples are high, only sample EA, with a loading level of 15.66% w/w, maintains good transparency. This phenomenon indicates that using ethanol-based LaF_3:Ce as doping material can effectively increase the nanoparticle loading levels within ORMOSILs, rendering a doping range between 15.66% and 27.09% w/w before LaF_3:Ce-doped ORMOSILs become opaque. By comparing those two sets of samples, it is seen that even though the concentration of LaF_3:Ce nanoparticles in ethanol is lower than in water, because of the larger ratio of ethanol than water during the sol-gel process, using ethanol-based LaF_3:Ce nanoparticles is an effective way to increase the nanoparticle loading level in ORMOSILs. Also, as described, during ORMOSIL synthesis, metal-containing clusters were incorporated into the ORMOSIL matrices by dissolving metal salts into the precursor solution prior to

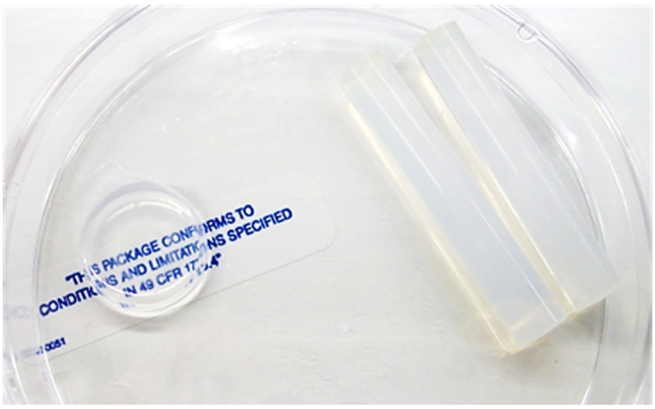

FIG. 1. Pure ORMOSIL samples with a good transparency.

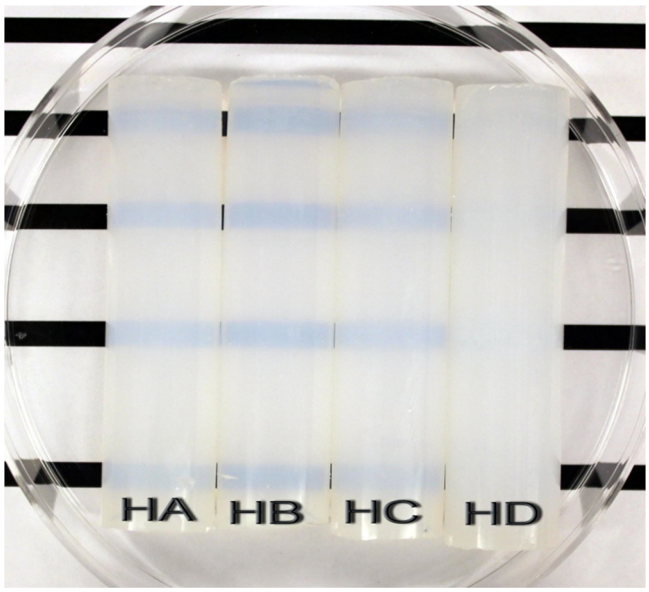

FIG. 2. Water-based LaF_3:Ce doped ORMOSILS with loading levels of HA—3.63%, HB—7.01%, HC—10.17%, and HD—13.11%.

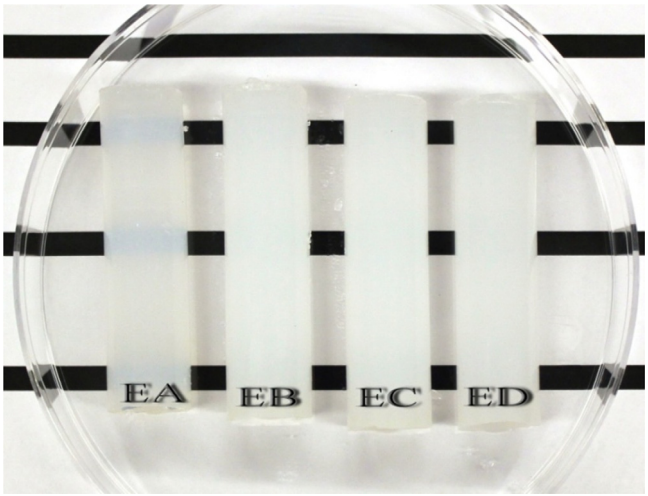

FIG. 3. Ethanol-based LaF_3:Ce doped ORMOSILS with loading levels of EA—15.66%, EB—27.09%, EC—35.78%, and ED—42.63%.

gelation. Using APTES as the organic source assists anchoring the dopant to the silica network, thereby avoiding precipitation of the salt.

Figure 4 shows the XRD pattern of ORMOSIL doped with ethanol-based LaF_3:Ce nanoparticles (EB, 27.09%) compared with that of pure LaF_3:Ce crystals. The results of the XRD are in good agreement with the trigonal tysonite LaF_3 structure as described in other reports,[27,28] and from bulk LaF_3 and CeF_3 crystals (JCPDS Card 32-0483 and 08-0045). No detectable signals of any impurity phase were observed; therefore, most likely Ce^{3+} has been doped into the LaF_3 crystal lattice. The ionic radius of Ce^{3+} (1.034 Å) is close to that of La^{3+} (1.061 Å), therefore, Ce^{3+} ions can substitute for La^{3+} ions in the LaF_3 crystal lattice. Based on the XRD results, nanoparticles maintain the same crystal structure after they are doped into ORMOSILs. Therefore, LaF_3:Ce doped ORMOSILs can be used for applications in radiation detection without loss in detection capability of the nanomaterial. The EELS of O *K*-edge and Si *K*-edge are

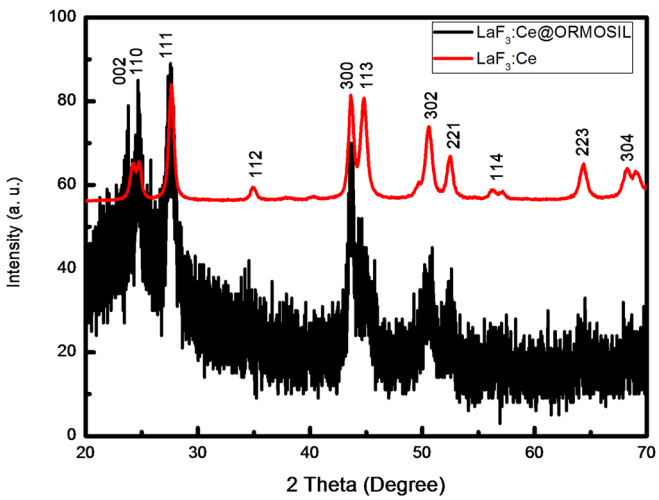

FIG. 4. XRD patterns of LaF_3:Ce and ethanol-based LaF_3:Ce doped ORMOSIL of EB—27.09%.

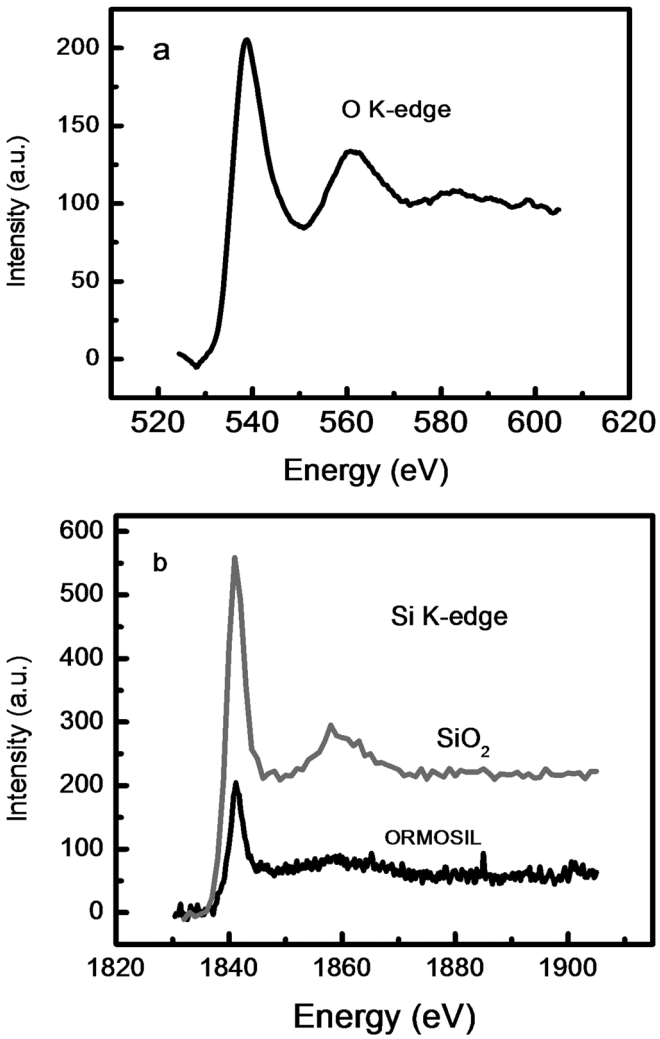

FIG. 5. The EELS of O *K*-edge (a) and Si *K*-edge (b) of pure ORMOSILs.

shown in Figure 5. Electron loss near-edge structure (ELNES) in the EELS spectrum contains the information of chemical bonding. Different shapes of ELNES for the same element show different chemical bonding. By comparing the experimental ELNES from ORMOSIL sample with the standard SiO_2 ELNES, ORMOSIL remains similar to SiO_2 in chemical characteristics. Additionally, SEM (Figure 6) shows the micromorphology of LaF_3:Ce-doped ORMOSILs. According to these micrographs, the open porosity of a typical ORMOSIL has not been compromised, and can be observed on the surface.

The porous structure of ORMOSILS can be seen in more detail in the high resolution TEM images displayed in Figure 7 for both pure ORMOSILs (top) and ORMOSILs doped with LaF_3:Ce nanoparticles (center and bottom). The pore size is around 5–10 nm and their distribution is not stereo-regular. The shape of LaF_3:Ce nanostructures is nanorod-like with about 5 nm in width and 10–15 nm in length. This is confirmed by HRTEM observations as shown in Figure 8. The interplanar spacing shown in Figures 2(a)–2(c) is about 3.5 Å along the [110] and [110] directions. These values are very close to the plane distance of 3.4 Å measured by X-ray diffraction. The result is also in

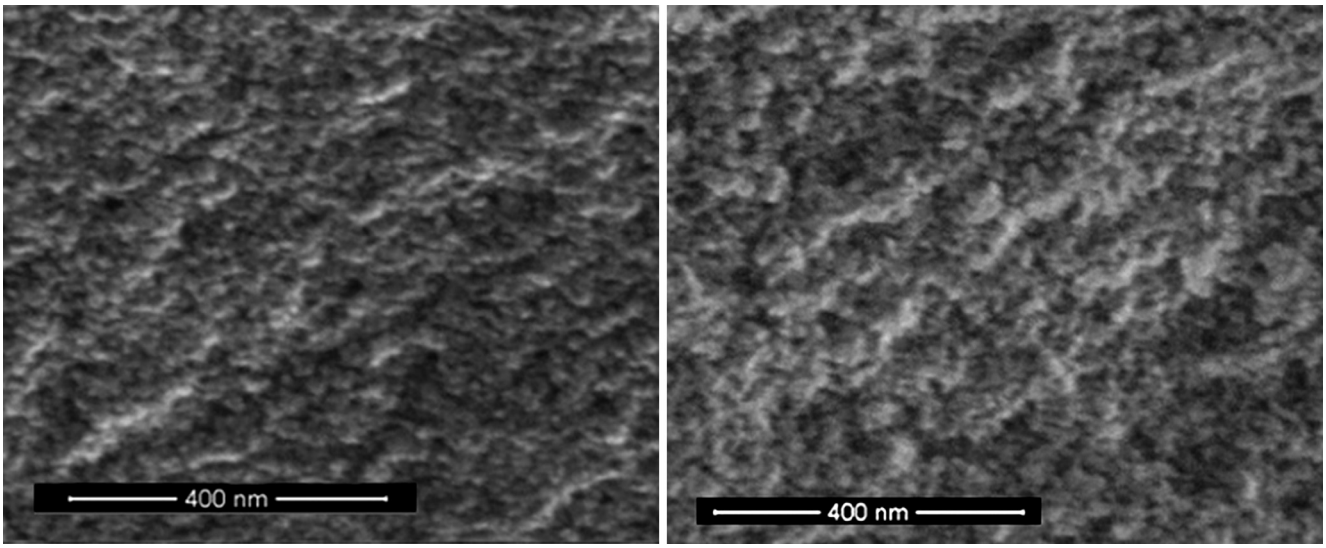

FIG. 6. SEM images of pure ORMOSIL (left) and water-based LaF_3:Ce doped ORMOSILS with a loading level HB—7.01%. (right).

agreement with the data concerning LaF_3 nanoplates.[29] The nanoparticles are very similar in shape to our previously reported LaF_3:Ce nanoparticles.[25,30] This means LaF_3:Ce nanoparticles maintain their structure and shape after encapsulation into ORMOSIL. The pore sizes and material densities measured for several representative samples are shown in Table I. Clearly, the pore sizes are smaller in the samples prepared using water soluble LaF_3:Ce than in the samples synthesized with ethanol soluble LaF_3:Ce.

Figure 9 shows typical stress-strain data for four nanoparticle filled silica aerogel specimens under compressive loading at room temperature. Mechanical data on the averages of the compressive strain at ultimate failure, Young's modulus, and the ultimate compressive strength are summarized in Table II. It is noted that the stress-strain relationships for the four samples of Table II are nearly linear up to failure so that it is sufficient to quote only their ultimate compressive strength. The small portion dropping-down past the maximum rise represents peeling-off at a small lateral surface region before final failure. It is observed that the ~5% compressive failure strain indicates a quasi-brittle behavior, not showing the three typical loading stages for polymer crosslinked silica aerogel: linearly elastic under small compressive strains (<4%), yield stage (until ~40% compressive strain), followed by densification and inelastic hardening.[14,15] Interestingly, samples did not exhibit significant lateral dilatation and did not buckle in compression. At failure, the outer layer of all samples shattered and fell away gradually, without any remaining cores, indicating that failure is due ultimately to lateral tensile stresses although the applied load is compressive.

Figure 10 shows emission spectra of LaF_3:Ce water-soluble nanoparticle doped ORMOSIL with different doping levels (HA-3.63%; HB-7.01%; HC-10.17%; HD-13.11%). ORMOSILs without doping display only very weak emission ($\lambda_{max} = 363$ nm). That phenomenon is similar to what has been reported by Kang and Kim,[31] in which TEOS with nitric acid under anhydrous conditions eliminates methyl formate instead of water during the sol-gel process;[32] the decomposition of ethyl formate can create substitutional defects, which are considered as the reason for the 363 nm emission. After doping with LaF_3:Ce nanoparticles, due to emission induced by the 5 d → 4f transition in the Ce^{3+} ions, all emission spectra are blue-shifted. The emission intensity increases with the doping level, reaching a maximum at 10.17% w/w of LaF_3:Ce. With a further increase of the doping level up to 13.11% w/w, no further increase in emission is observed (see inset in Figure 10).

Figure 11 shows the emission spectra of ORMOSILs doped with ethanol-based LaF_3:Ce nanoparticles at different doping levels (EA-15.66% w/w, EB-27.09% w/w, EC-35.78% w/w; and, ED-42.63% w/w). Similar to the emissions of those ORMOSILs doped with water-based nanoparticles, all emission spectra have been blue-shifted compared with the defect emission of ORMOSILs without doping. Comparing the emissions of ORMOSILs with different nanoparticle doping concentrations, it has been found that the emission intensities first increased and then decreased with a maximum at a doping concentration of 27.09% w/w (see inset in Figure 11). For higher loadings, the luminescence intensity should be stronger. However, at high loadings, nanoparticles may aggregate and the nanocomposites may lose their transparency, so the apparent luminescence efficiency is decreased.

As a first step to test LaF_3:Ce doped ORMOSILs for radiation detection, we investigated the photoluminescence under X-ray excitation (Figure 12) for doped ORMOSILs as those shown in Figure 3. Under those conditions, luminescence is observed with two peaks at 335 nm and 400 nm. The 335 nm emission originates from the 5 d → 4f transitions of Ce^{3+}, while the 400 nm emission source is the so-called self-trapped excitons (STE).[33,34] The STE emission is observed during X-ray excitation, but not in UV-excited photoluminescence, because more excitons are produced by high-energy X-rays than by UV light. The excitons are trapped by Ce^{3+} to form STE.[33,34] The variation of the X-ray-excited

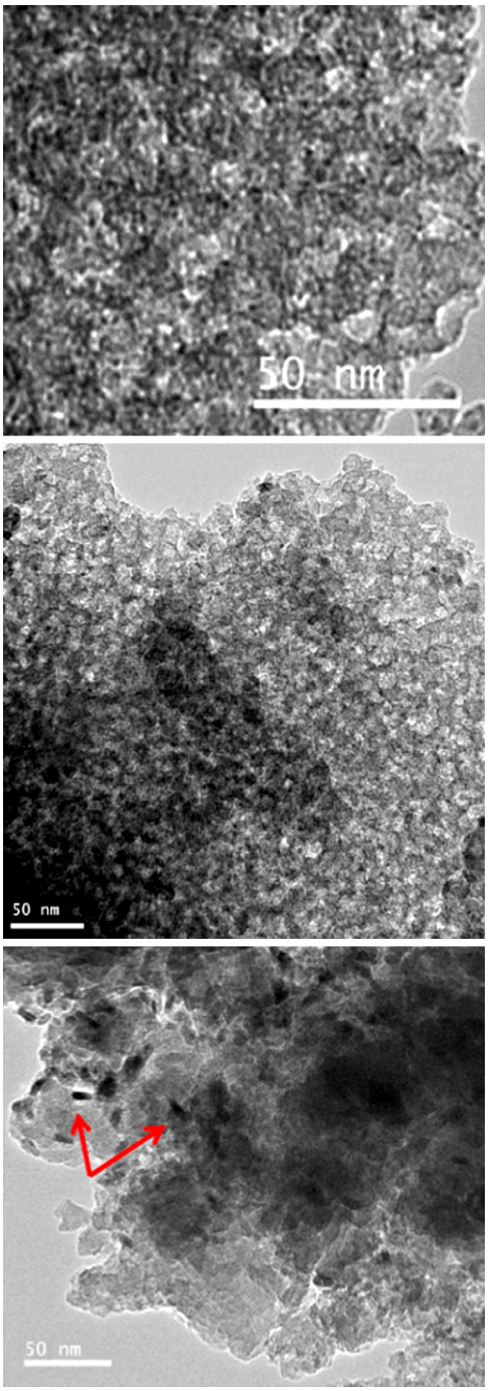

FIG. 7. TEM images of pure ORMOSIL (top) and water-based LaF_3:Ce doped ORMOSILS with loading level HB—7.01% (middle and bottom). The red arrows indicate the LaF_3:Ce nanoparticles in ORMOSIL.

TABLE I. Pore sizes and densities of ORMOSILs.

Sample	HA	HB	HD	EA	EB
Particle radius (nm)	3.71	3.05	11.80	15.10	10.5
BET surface area, σ (m^2/g)	491.24	603.8	152.76	122.28	176.42
Pore size by $4 \times V_{Total}/\sigma$ method	8.5 nm	4.9 nm	7.2 nm	12.9 nm	12.6 nm
Pore size by BJH-absorption	9.3 nm	8.0 nm	8.0 nm	13.7 nm	13.6 nm
Pore size by BJH desorption	5.8 nm	4.0 nm	4.1 nm	8.1 nm	8.3 nm
Average density (g/cm^3)	1.6478	1.6176	1.6625	1.6215	1.6176

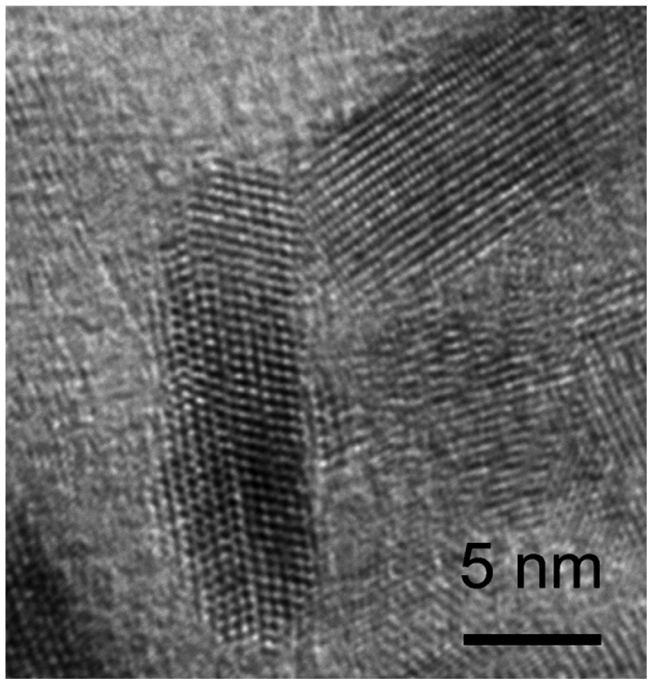

FIG. 8. High resolution TEM image of water-based LaF_3:Ce doped ORMOSILS with a loading level HB—7.01%. The LaF_3:Ce nanorods are about 5 nm wide and 5–10 nm long.

luminescence intensity with the nanoparticle loading level is shown in the inset of Figure 12, and is similar to that of UV-excited photoluminescence as displayed in the inset of Figure 11. The observation of strong photoluminescence from LaF_3:Ce-doped ORMOSILs by X-ray excitation suggests that those nanocomposites have tremendous potential for radiation detection, even though challenging issues such as how to increase the nanoparticle loading level while maintaining good transparency need to be resolved, and are under investigation.

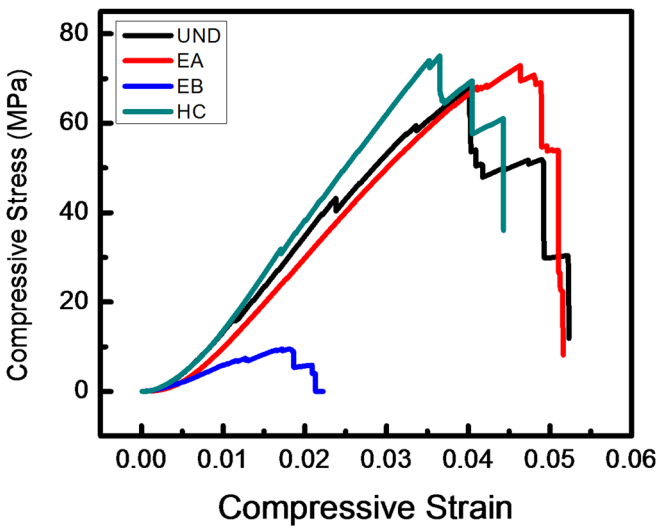

FIG. 9. Typical compressive stress-strain curves of ethanol-based LaF_3:Ce doped ORMOSILS with loading levels of 0% (UND), EA-15.66%, EB-27.09%, and water-based LaF_3:Ce doped ORMOSILS with a loading levels of HC-10.17%.

TABLE II. Summary of compressive properties of ORMOSIL at a low strain rate.

Sample	Size (mm)	Strain rate (/s)	Failure strain (%)	Compressive strength (MPa)	Modulus E (GPa)
UND	$\phi 5.84 \times 9.60$	0.0002	4.02	67.9	2.18
EA	$\phi 6.02 \times 9.68$	0.0002	4.63	72.8	2.03
EB	$\phi 6.53 \times 18.21$	0.0002	1.83	9.48	0.79
HC	$\phi 7.11 \times 12.24$	0.0002	3.64	74.9	2.42

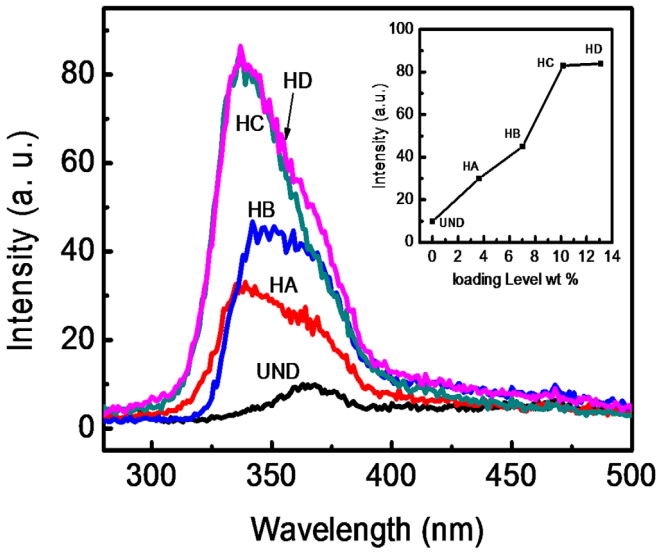

FIG. 10. Photoluminescence emission spectra of water-based LaF_3:Ce doped ORMOSILS with loading levels of UND—0%, HA—3.63%, HB—7.01%, HC—10.17%, and HD—13.11%. The inset is the luminescence intensity change with the nanoparticle loading levels. The excitation wavelength is 280 nm.

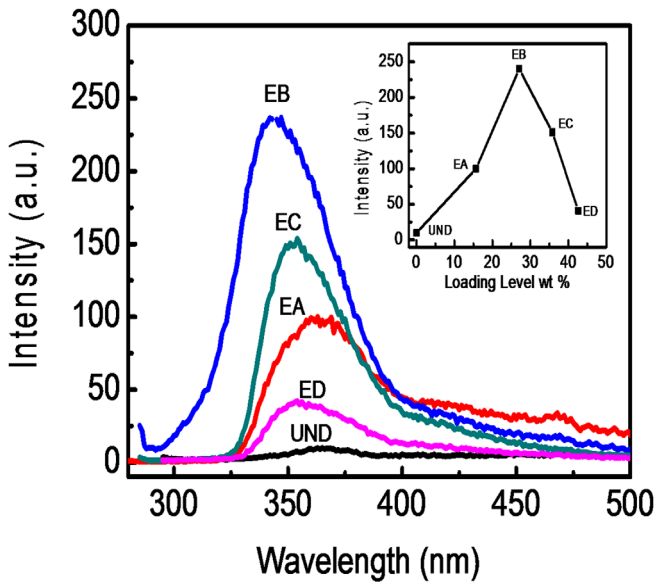

FIG. 11. Photoluminescence emission spectra of ethanol-based LaF_3:Ce doped ORMOSILS with loading levels of UND—0%, EA—15.66%, EB—27.09%, EC—35.78%, and ED—42.63%. The inset is the luminescence intensity change with the nanoparticle loading levels. The excitation wavelength is 280 nm.

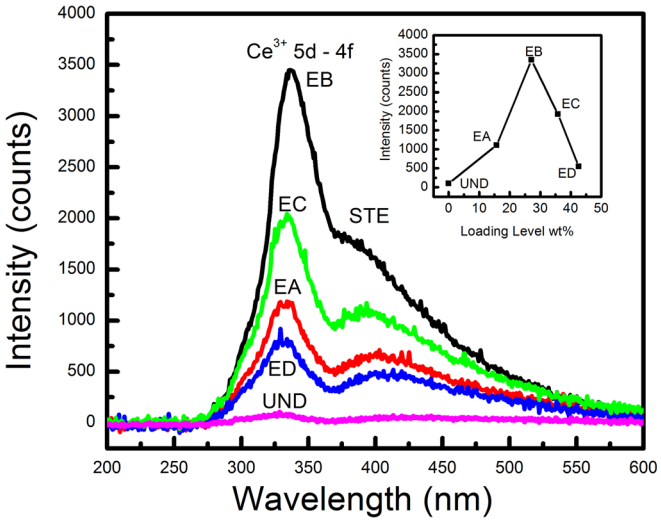

FIG. 12. X-ray luminescence of ethanol-based LaF_3:Ce doped ORMOSILS with loading levels of UND–0%, EA—15.66%, EB—27.09%, EC—35.78%, and ED—42.63%. The inset is the luminescence intensity change with the nanoparticle loading levels.

IV. CONCLUSIONS

In summary, for the first time, LaF_3:Ce nanoparticle-doped ORMOSILs are synthesized by a sol-gel process, using amine-functionalized APTES and TMOS, and their structure and optical properties are investigated. Thus, doped ORMOSILs display intense photoluminescence excited either by UV or X-rays, and maintain good transparency at a loading level of up to 15.66% w/w. TEM demonstrates that doping does not compromise the porosity of regular ORMOSILs with pore diameters in the 5–10 nm range. LaF_3:Ce nanoparticles in doped ORMOSILs are rod-like, 5 nm in diameter and 10–15 nm in length. Compression testing indicates that the nanocomposites have very good strength and overall have potential for applications in radiation detection and solid-state lighting.

ACKNOWLEDGMENTS

We would like to recognize support from the NSF and DHS joint ARI program (2011-DN-077-ARI053-02&3), and the U.S. Army Medical Research Acquisition Activity (USAMRAA) under Contract Nos. W81XWH-10-1-0279 and W81XWH-10-1-0234. Luo and Lu also acknowledge the support of NSF under DMR-0907291, CMMI-1031829, and CMMI-1132174. Leventis acknowledges support from ARO under Award No. W911NF-10-1-0476.

[1]S. E. Derenzo, M. J. Weber, E. Bourret-Courchesne, and M. K. Klintenberg, Nucl. Instrum. Methods Phys. Res. A **505**, 111–117 (2003).
[2]W. Chen, J. Nanosci. Nanotechnol. **8**, 1019–1051 (2008).
[3]W. Chen, J. Z. Zhang, and A. G. Joly, J. Nanosci. Nanotechnol. **4**, 919–947 (2004).
[4]W. Chen, X. Zhang, and Y. Huang, Appl. Phys. Lett **76**, 2328–2330 (2000).
[5]Y. Liu, Q. Ju, and X. Chen, Rev. Nanosci. Nanotechnol. **1**, 163–171 (2012).
[6]E. A. McKigney, R. E. D. Sesto, L. G. Jacobsohn, P. A. Santi, R. E. Muenchausen, K. C. Ott, T. M. McCleskey, B. L. Bennett, J. F. Smith, and D. W. Cooke, Nucl. Instrum. Methods Phys. Res. A **579**, 15–18 (2007).

[7]S. E. Letant and T.-F. Wang, Nano Lett. **6**, 2877 (2006).
[8]M. F. Bertino and L. Franzel, Rev. Nanosci. Nanotechnol. **1**, 52–56 (2012).
[9]D. Avnir, Acc. Chem. Res. **28**, 328–334 (1995).
[10]C. J. Brinker, J. Non-Cryst. Solids **100**, 31–50 (1988).
[11]M. F. Bertino, R. R. Gadipalli, L. A. Martin, L. E. Rich, A. Yamilov, B. R. Heckman, N. Leventis, S. Guha, J. Katsoudas, R. Divan, and D. C. Mancini, Nanotechnology **18**, 315603 (2007).
[12]M. F. Bertino, R. R. Gadipalli, L. A. Martin, J. G. Story, B. Heckman, S. Guha, and N. Leventis, J. Sol-Gel Sci. Technol. **39**, 299–306 (2006).
[13]R. R. Gadipalli, L. A. Martin, B. Heckman, J. G. Story, M. F. Bertino, P. Fraundorf, S. Guha, and N. Leventis, J. Sol-Gel Sci. Technol. **40**, 101–107 (2006).
[14]A. Katti, N. Shimpi, S. Roy, H. Lu, E. F. Fabrizio, A. Dass, L. A. Capadona, and N. Leventis, Chem. Mater. **18**, 285–296 (2006).
[15]N. Leventis, Acc. Chem. Res. **40**, 874–884 (2007).
[16]L. Guo, J. H. Lee, and G. Beaucage, J. Non-Cryst. Solids **243**, 61 (1999).
[17]M. M. Collinson and A. R. Howells, Anal. Chem. **72**, 702A–709A (2000).
[18]T. Jin, S. Inoue, S. Tsutsumi, K. Machida, and G. Adachi, J. Non-Cryst. Solids **223**, 123–132 (1998).
[19]M. D. Birowosuto, P. Dorenbos, C. W. E. v. Eijk, K. W. Kramer, and H. U. Gudel, IEEE Trans. Nucl. Sci. **52**, 1114–1118 (2005).
[20]R. Kasuya and T. Isobe, J. Phys. Chem. B **109**, 22126–22130 (2005).
[21]N. M. Khaidukova, S. K. Lamb, D. Lob, and V. N. Makhov, Opt. Commun. **205**, 415–420 (2005).
[22]C. Pedrinit, B. Moinet, J. C. Gacon, and B. Jacquier, J. Phys: Condens. Matter **4**, 5461 (1992).
[23]E. Radzhabov, Radiat. Eff. Defects Solids **158**, 203–207 (2003).
[24]B. K. Woo, A. G. Joly, and W. Chen, J. Lumin. **131**, 49–53 (2011).
[25]M. Yao, A. G. Joly, and W. Chen, J. Phys. Chem. C. **114**, 826–831 (2010).
[26]M. S. Zhang, J. Yu, W. C. Chen, and Z. Yin, Prog. Cryst. Growth Charact. Mater. **40**, 33–42 (2000).
[27]W. Chen, J. Zhang, S. L. Westcott, A. G. Joly, J.-O. Malm, and J.-O. Bovin, J. Appl. Phys. **99**, 34302 (2006).
[28]N. Gaponik, D. V. Talapin, A. L. Rogach, K. Hoppe, E. V. Shevchenko, A. Kornowski, A. Eychmuller, and H. Weller, J. Phys. Chem. B **106**, 7177–7185 (2002).
[29]Y. W. Zhang, X. Sun, R. Si, L. P. You, and C. H. Yan, J. Am. Chem. Soc. **127**, 3260 (2005).
[30]M. Yao, X. Zhang, L. Ma, W. Chen, A. G. July, J. Huang, and Q. Wang, J. Appl. Phys. **108**, 103104 (2010).
[31]K. S. Kang and J. H. Kim, J. Phys. Chem. C. **112**, 618–620 (2008).
[32]W. H. Green, K. P. Le, J. Grey, T. T. Au, and M. J. Sailor, Science **276**, 1826–1828 (1997).
[33]P. Dorenbos, Phys. Status Solidi A **202**, 195–200 (2005).
[34]K. W. Kramer, P. Dorenbos, H. U. Gudel, and C. W. E. v. Eijk, J. Mater. Chem. **16**, 2773–2780 (2006).